Controlled Photoinduced Electron Transfer via Triplet in Polymer Matrix Using Electrostatic Interactions

Yilin CAO [a], Hikaru SOTOME [b], Yuichiro KOBAYASHI [a,c,d], Syoji ITO [b,e], Hiroyasu YAMAGUCHI [a,c,d,*]

a Department of Macromolecular Science, Graduate School of Science, Osaka University, 1-1 Machikaneyama, Toyonaka, Osaka 560-0043, Japan
b Division of Frontier Materials Science, Graduate School of Engineering Science, Osaka University, Toyonaka, Osaka 560-8531, Japan
c Innovative Catalysis Science Division, Institute for Open and Transdisciplinary Research Initiatives (ICS-OTRI), Osaka University, Suita, Osaka 567-0871, Japan
d Project Research Center for Fundamental Sciences, Graduate School of Science, Osaka University, Toyonaka, Osaka 560-0043, Japan
e Research Institute for Light-induced Acceleration System (RILACS), Osaka Metropolitan University, 1-2, Gakuen-cho, Naka-ku, Sakai, Osaka 599-8570, Japan

Abstract

Drawing inspiration from highly efficient natural photosynthetic systems, we developed an artificial photoinduced electron transfer (PET) system within a poly(*N*-methyl-4-vinylpyridinium) (P4VPMe) polymer matrix. This system features 5,10,15,20-tetrakis-(4-sulfonatophenyl) porphyrin (TPPS) and its zinc complex (ZnTPPS) as electron donors and methylviologen (MV^{2+}) as the electron acceptor. In the presence of an excess of P4VPMe, ZnTPPS exists as individual molecules rather than self-aggregating, favoring PET. Under these conditions, P4VPMe inhibits the formation of ground-state charge-transfer complex between ZnTPPS and MV^{2+}. This shifts the main PET process from singlet to triplet states. ZnTPPS in an excess of P4VPMe demonstrates over a tenfold increase in catalytic activity for the photoinduced oxidation of MV^{2+} compared to ZnTPPS alone.

Keywords: photoinduced electron transfer; water-soluble porphyrin; polymer matrix; porphyrin aggregates.

Introduction

In recent years, the study of electron transfer processes within complex molecular systems has garnered increasing attention due to its pivotal role in a wide range of scientific and technological applications [1–4]. Among the diverse array of molecular systems, porphyrins have emerged as fascinating candidates for exploring electron transfer dynamics. These aromatic macrocycles exhibit

unique photophysical properties, making them ideal platforms for investigating charge transfer and energy transfer phenomena [5,6].

In particular, the interaction between porphyrins and various electron acceptors within a polymer matrix has captured the interest of researchers seeking to understand and control these processes [7–12]. These systems' potential applications span diverse fields, including photovoltaics [13–15], sensors [16,17], and molecular electronics [18,19].

This study delves into the intricate electron transfer dynamics within a porphyrin (TPPS and ZnTPPS), polymer (P4VPMe), and electron acceptor (MV^{2+}) system, with a focus on the role of the polymer matrix in modulating these interactions (Fig. 1). P4VPMe polymer matrix refers to the solution environment created by the cationic, amphiphilic polymer P4VPMe, which is dispersed throughout the solution. By gaining insights into the electron transfer processes and their modulation, we hope to contribute to the development of advanced materials and technologies [20–22].

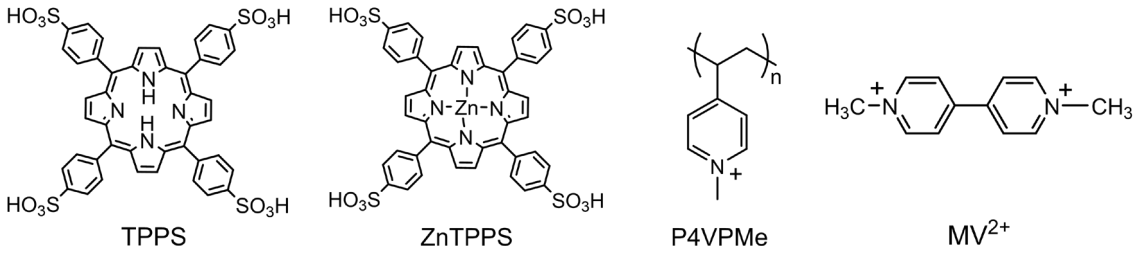

Fig. 1. Chemical structures of TPPS, ZnTPPS, P4VPMe and MV^{2+}.

Result and Discussion

Evolution of Porphyrin Aggregates in P4VPMe Polymer Matrix

To investigate the changes of ZnTPPS when interact with P4VPMe, absorption spectra of mixed solutions of ZnTPPS and P4VPMe (M_n = 4,300) at different charge ratios (I = c_{charge}(porphryin) / c_{charge}(P4VPMe)) in a 0.01 M phosphate buffer (pH = 8.0) were recorded. The Soret band of ZnTPPS, with a maximum absorption at 420 nm, exhibited a redshift upon the addition of P4VPMe (I = 0.10) and broadened into a multi-component band, displaying peaks at 410 nm, 430 nm, and 440 nm simultaneously (Fig. 2a). Further addition of P4VPMe led to an increase in absorbance at 430 nm and a decrease in absorbance at 410 nm and 440 nm. Ultimately, in the presence of an excess of P4VPMe (I = 0.01), a single-component band at 430 nm was observed.

Excitation spectra (λ_{em} = 605 nm) of these mixed solutions were recorded to identify the components that appeared during the addition of P4VPMe. When ZnTPPS was irradiated at 420 nm, it emitted at 605 nm when in isolation. However, in the presence of P4VPMe, ZnTPPS emitted light only when irradiated at 430 nm, regardless of the quantity of P4VPMe added (Fig. 2b). Therefore, the component with a 430 nm absorption was identified as a single molecule of ZnTPPS within the P4VPMe polymer

matrix, while the other components at 410 nm and 440 nm were determined to be (J or H) aggregates of ZnTPPS within the P4VPMe polymer matrix [23,24].

It can be concluded that, as the addition of P4VPMe progressed, ZnTPPS initially formed aggregates at low P4VPMe concentrations. Subsequently, these aggregates gradually dissociated into individual ZnTPPS molecules as the P4VPMe reached an excess amount (Fig. 3a), as illustrated in the spectral data and discussed in Figs. 2a and 2b. Furthermore, the aggregation and dissociation of ZnTPPS in the P4VPMe polymer matrix were also examined and supported by excited singlet lifetime measurements of ZnTPPS with P4VPMe (upon the addition of P4VPMe, the singlet lifetime of ZnTPPS initially decreased and then recovered in the presence of an excess of P4VPMe; see Table 1).

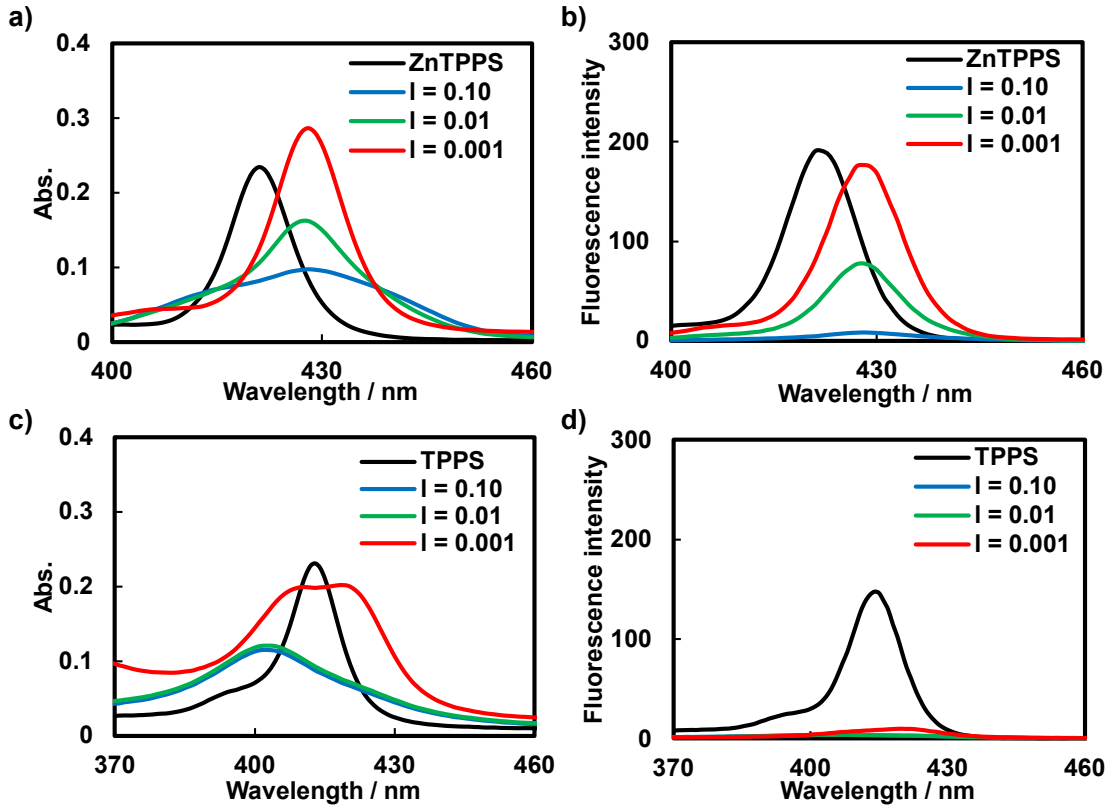

Fig. 2. Absorption spectra of mixing solutions of P4VPMe and 0.6 μM a) ZnTPPS or c) TPPS at various charge ratios (I = 0.10, 0.01 and 0.001) in 0.01 M phosphate buffer (pH = 8.0). Excitation spectra of mixing solutions of P4VPMe and 0.6 μM b) ZnTPPS (λ_{em} = 605 nm) or d) TPPS (λ_{em} = 640 nm) at various charge ratios (I = 0.10, 0.01 and 0.001) in 0.01 M phosphate buffer (pH = 8.0).

Absorption spectra and excitation spectra (λ_{em} = 640 nm) of mixed solutions of TPPS and P4VPMe at different I in a 0.01M phosphate buffer (pH = 8.0) were also recorded. Notable changes, such as shifting and broadening, were observed in the Soret band of TPPS upon the addition of P4VPMe (Fig.

2c). However, none of these changes resulted in obvious emission (Fig. 2d). This suggests that TPPS forms aggregates when mixed with P4VPMe, and these aggregates persist even in the presence of an excess of P4VPMe (Fig. 3b). The aggregation of TPPS in the P4VPMe polymer matrix was further confirmed through excited singlet lifetime measurements. With the addition of P4VPMe, the lifetime of TPPS consistently decreased in one direction (Table 1), providing additional evidence for the formation of TPPS aggregates within the P4VPMe polymer matrix.

The difference in aggregation behavior primarily stems from the intrinsic structural and chemical differences between ZnTPPS and TPPS. The incorporation of zinc enhances the rigidity of the porphyrin ring in ZnTPPS, reducing its flexibility for self-aggregation. This rigidity, coupled with zinc's axial coordination with solvent molecules, significantly reduces ZnTPPS's tendency to self-aggregate [25, 26]. At high P4VPMe concentrations, the charges on TPPS molecules are neutralized, reducing intermolecular electrostatic repulsion and thus making TPPS more prone to self-aggregation. This behavior is attributed to the weakening of electrostatic repulsion between the rings, making the inherent aggregative properties of TPPS more pronounced.

Table 1. Excited singlet-state lifetimes, τ_i (i = 1–4), of ZnTPPS and TPPS in the absence and presence of P4VPMe. A_i (i = 1–4) are corresponding pre-exponential factors in % and τ_{avg} is averaged lifetime.

Sample	τ_1 / ns	τ_2 / ns	τ_3 / ns	τ_4 / ns	A_1	A_2	A_3	A_4	τ_{avg} / ns
ZnTPPS	1.88				100				1.88
I = 0.10	0.092	0.470	1.62	3.20	69	12	17	2	0.459
I = 0.01	0.289	1.34	2.17		14	44	42		1.54
I = 0.001	0.656	1.50	2.04		18	57	25		1.48
TPPS	10.0				100				10.0
I = 0.10	0.464	2.38	10.8		29	33	38		5.02
I = 0.01	0.472	2.16	9.10		33	46	21		3.06
I = 0.001	0.344	1.80	4.96		37	43	20		1.89

The average lifetime was defined as pre-exponential factor-weighted average (first moment) and described by equation: $\tau_{\text{avg}} = \frac{\sum_{i=1}^{4} A_i \tau_i}{\sum_{i=1}^{4} A_i}$

In the polymer matrix, ZnTPPS or TPPS molecules are present as the aggregates in slightly different environments reflected by interactions with the heterogeneous matrix, and the individual molecules have distinct fluorescence lifetimes from each other. We consider that these heterogeneous environment and aggregation manner are distributed continuously rather than with four specific environments because the lifetime of each component varies with change of the charge ratio, as shown in Table 1.

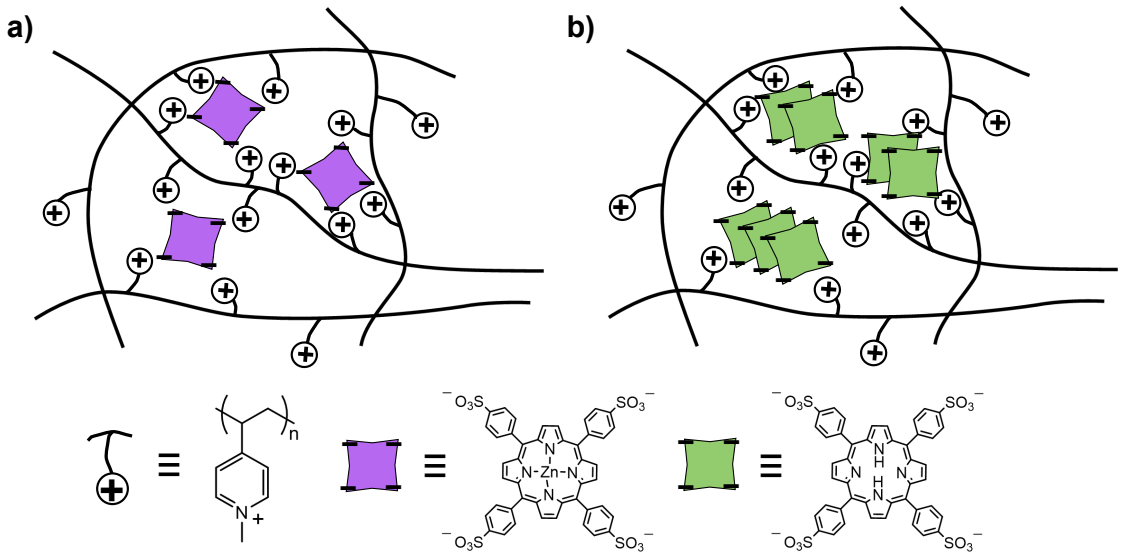

Fig. 3. Conceptual figures of a) ZnTPPS exists as individual molecule and b) TPPS forms aggregates in excess of P4VPMe.

Charge-transfer complex and photoinduced electron transfer

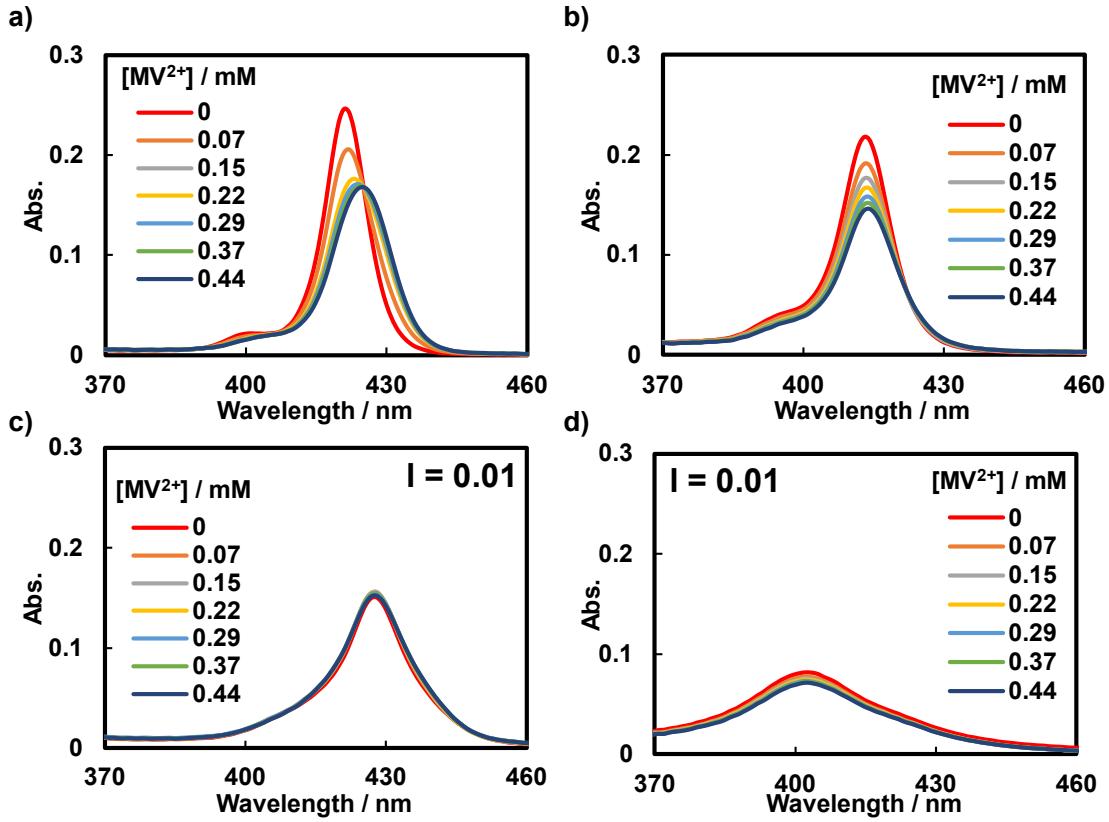

Fig. 4. Absorption spectra of 0.6 μM a) ZnTPPS and b) TPPS upon the addition of MV^{2+} in 0.01 M phosphate buffer (pH = 8.0). Absorption spectra of 0.6 μM c) ZnTPPS and d) TPPS upon the addition of MV^{2+} in the presence of P4VPMe (I = 0.01) in 0.01 M phosphate buffer (pH = 8.0). Concentrations of added MV^{2+} are indicated in the figures.

ZnTPPS and TPPS are recognized for their ability to form charge-transfer complex with MV^{2+} [27]. When MV^{2+} is introduced, both ZnTPPS and TPPS exhibit a notable shift in their Soret bands towards longer wavelengths (Figs. 4a and 4b), indicating the formation of charge-transfer complex. However, in the presence of P4VPMe (I = 0.01), minimal changes were observed in the Soret bands of either ZnTPPS or TPPS upon the addition of MV^{2+} (Figs. 4c and 4d). This suggests that P4VPMe exerts a restraining influence on the formation of ground-state charge-transfer complex between ZnTPPS or TPPS and MV^{2+}.

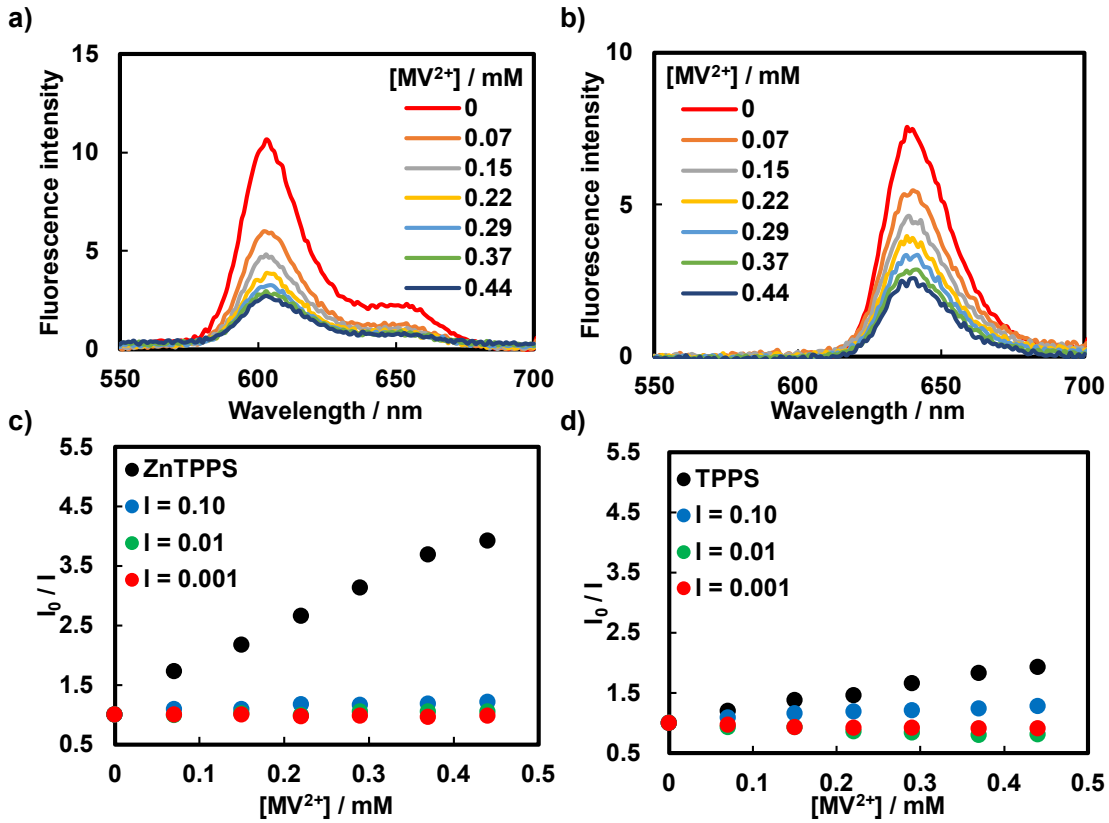

Fig. 5. Florescence spectra of 0.6 μM a) ZnTPPS and b) TPPS upon the addition of MV^{2+} in air-saturated 0.01M phosphate buffer (pH = 8.0). Concentrations of added MV^{2+} are indicated in the figures. Stern-Volmer plots for the quenching of c) ZnTPPS and d) TPPS by MV^{2+} in the absence and presence of P4VPMe at different charge ratios.

The addition of MV^{2+} led to a reduction in the fluorescence intensity of ZnTPPS and TPPS (Figs. 5a and 5b), a phenomenon commonly referred to as fluorescence quenching. This quenching is attributed to the electron transfer from the excited singlet state of ZnTPPS or TPPS to MV^{2+}. Fluorescence quenching experiments involving ZnTPPS and TPPS in the presence of P4VPMe in the air were also conducted, and Stern-Volmer plots were constructed based on the fluorescence intensities (Figs. 5c, and 5d). The slopes of the Stern-Volmer plots, represented as Stern-Volmer constants (K_{SV}), decreased for both ZnTPPS and TPPS systems following the addition of P4VPMe. This observation suggests that the presence of P4VPMe creates a less favorable environment for PET, aligning with the results obtained from absorption spectra which showed a restriction in the formation of ground-state charge-transfer complex. In the case of TPPS, K_{SV} values became negative in the presence of an excess of P4VPMe (I = 0.01 and 0.001). This phenomenon was attributed to the minor partial dissociation of TPPS aggregates within the P4VPMe polymer matrix induced by the addition of MV^{2+}, resulting in a slight increase in fluorescence intensity.

Fluorescence lifetimes of ZnTPPS and TPPS within the polymer matrix become slightly shorter with the addition of MV^{2+} (Table S1). This result indicates that a small fraction of ZnTPPS and TPPS in the S_1 state undergoes electron transfer to MV^{2+} although the rapid recombination of the charge-separated state may take place in the early time stage, not significantly contributing to the catalytic process in the later time region.

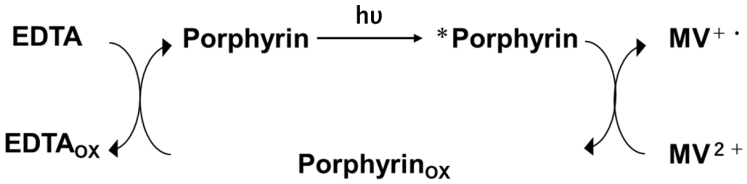

Scheme 1. Generation of $MV^{+\bullet}$ from MV^{2+} via electron transfer from photoexcited porphyrin with EDTA as a sacrificial agent.

Ethylenediamine-*N*,*N*,*N*′,*N*′-tetraacetic acid tetrasodium salt (EDTA) was introduced as a sacrificial agent to enable the reduction of oxidized ZnTPPS or TPPS after the PET process (Scheme 1). This allowed for continuous PET experiments to be conducted. Deoxygenated solutions containing ZnTPPS or TPPS, P4VPMe, MV^{2+}, and EDTA were exposed to light ($\lambda > 400$ nm) at an intensity of ca. 3 $mWcm^{-2}$ for a duration of 30 minutes. The quantities of generated methylviologen cation radical ($MV^{+\bullet}$) were determined by monitoring changes in absorbance at 605 nm, a characteristic absorption wavelength of $MV^{+\bullet}$, in conjunction with its molar absorption coefficient (Fig. 6) [28].

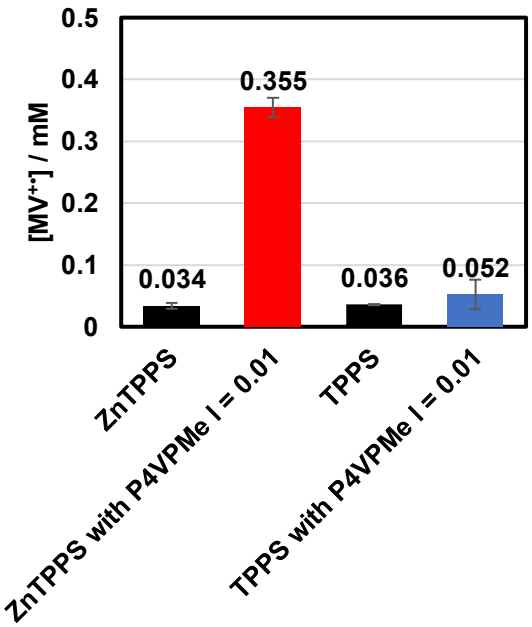

Fig. 6. Generated concentrations of $MV^{+\bullet}$ in ZnTPPS and TPPS systems, in the absence and presence

of P4VPMe.

Conversions of MV^{2+} to $MV^{+\bullet}$ during the reaction were 3.4% for ZnTPPS and 35.5% for ZnTPPS with P4VPMe (I = 0.01). Those for TPPS and TPPS with P4VPMe (I = 0.01) were 3.6% and 5.2%, respectively. Within the P4VPMe polymer matrix, ZnTPPS exhibited over a tenfold increase in the generation of $MV^{+\bullet}$ compared to ZnTPPS alone, without P4VPMe. In contrast, the catalytic activity for the photoinduced oxidation of MV^{2+} by TPPS remained relatively unchanged in the presence or absence of P4VPMe. This difference can be attributed to the distinct aggregate states of ZnTPPS and TPPS within P4VPMe. The aggregation states within the polymer matrix play a crucial role in this variation. When aggregated, absorbed photon energy tends to dissipate as thermal energy rather than participating in PET.

In addressing the role of the charge ratio (I) in determining the yield of the methylviologen radical cation ($MV^{+\bullet}$) for ZnTPPS and TPPS, we observed distinct optima: I = 0.01 for ZnTPPS and I = 0.001 for TPPS (Fig. S21). The optimal yield of $MV^{+\bullet}$ in the ZnTPPS system at I = 0.01 is attributed to the disassociation of ZnTPPS aggregates into monomers facilitated by increased P4VPMe concentration, enhancing photoinduced electron transfer (PET). However, an excessive P4VPMe concentration introduces a strong electrostatic repulsion, hindering MV^{2+}'s approach to ZnTPPS, thus defining the observed optimal yield. For TPPS, the highest yield of $MV^{+\bullet}$ at I = 0.001 corresponds to the initial stages of TPPS disassociation into monomers. A further increase in P4VPMe concentration is expected to produce a yield peak for TPPS as well, due to a similar interplay of disassociation and electrostatic repulsion effects.

Although ZnTPPS exists as individual molecule within the P4VPMe matrix, favoring the PET process, it predominantly occurs from the singlet excited state. However, the PET process from the singlet state results in a minimal generation of $MV^{+\bullet}$, as evidenced by the near-zero K_{SV}, indicating only a limited electron transfer from the singlet state of ZnTPPS to MV^{2+}. The primary PET pathway in this system may involve the triplet state under deoxygenated conditions. To investigate this process, transient absorption spectra were recorded.

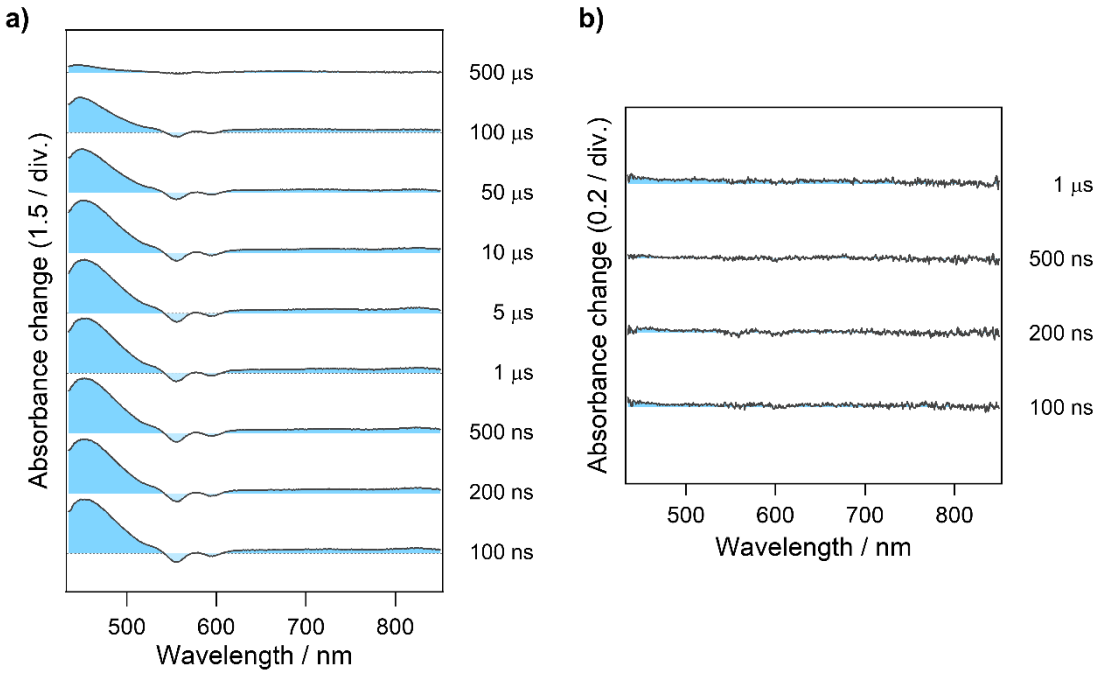

Fig. 7. Transient absorption spectra of a) ZnTPPS and b) ZnTPPS with MV^{2+} in the nanosecond and microsecond time regions. The sample solution was treated with nitrogen bubbling before the measurements.

For ZnTPPS, an absorption band originating from the triplet state of the ZnTPPS is observed approximately 100 ns after photoexcitation, appearing in the region below 540 nm (Fig. 7a). This characteristic band persists for several hundreds of microseconds before showing partial decay at around 500 µs, corresponding to the intrinsic triplet state lifetime of ZnTPPS [29]. However, when MV^{2+} is introduced to this ZnTPPS system, no transient absorption signals are detected (Fig. 7b). In this scenario, even if a charge-transfer state is formed after photoexcitation, it rapidly recombines to the ground state. The charge recombination takes place with a time constant of 700 fs [30]. Thus, the $MV^{+\bullet}$ absorption is not observed in the transient absorption spectra in the nanosecond and microsecond time regions within the temporal resolution of the current measurement.

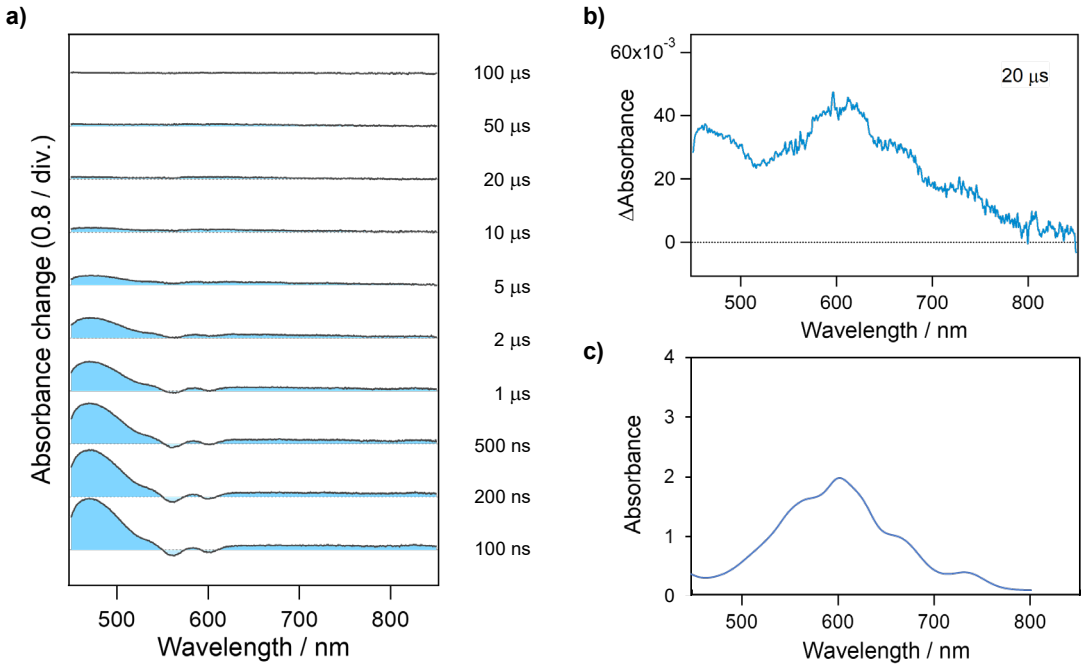

Fig. 8. a) Transient absorption spectra of mixing solution of ZnTPPS, MV^{2+}, and P4VPMe in the nanosecond and microsecond time regions. b) Enlarged spectrum recorded at 20 µs. The sample solution was treated with nitrogen bubbling before the measurements. c) Absorption spectrum of $MV^{+\bullet}$.

In the ZnTPPS, P4VPMe, and MV^{2+} system, the triplet absorption band of porphyrin is initially observed upon excitation and decays over a time scale of a few microseconds (Fig. 8a). Additionally, upon further enlargement of the transient absorption spectrum after this time, the appearance of the $MV^{+\bullet}$ absorption band, believed to be generated by electron transfer, is detected (Figs. 8b and 8c). The absorption band due to $MV^{+\bullet}$ almost vanished at 100 µs after the photoexcitation. Thus, we estimated the lifetime of $MV^{+\bullet}$ to be < 100 µs. It should be noted that this $MV^{+\bullet}$ absorption band was not observed under the air-saturated condition where molecular oxygen effectively quenches the triplet state (Fig. S23b). This observation strongly suggests that electron transfer from the triplet state of ZnTPPS to MV^{2+} is indeed occurring.

We evaluated the quantum yield of electron transfer in following two methods. The details are shown in the Supporting Information (Figure S24, S25). In the first method, the quantum yield was estimated to be 0.97 from shortening of the lifetime of ZnTPPS in the T_1 state with the addition of MV^{2+}, that is, quenching experiments. But it should be noted that the absorption band of $MV^{+\bullet}$ produced by electron transfer is rather small (Fig. 8). To verify this result, we next estimated the production yield of $MV^{+\bullet}$ from the amounts of the reactant (ZnTPPS in the T_1 state) and product ($MV^{+\bullet}$). The yield was evaluated as 0.27, which is significantly lower than the value obtained from the first method (0.97). These results indicate that a fraction of the charge-separated state undergoes the rapid recombination probably due

to its short pair distance. We adopted the value of 0.27 as the quantum yield of electron transfer because the remaining charge-separated state free from the rapid recombination is available for the subsequent catalytic process.

As clearly in the above evaluation of the electron transfer yield, a key factor in the increase of the catalytic activity is suppression of the charge recombination by increase of the donor (ZnTPPS)-acceptor (MV^{2+}) distance in the presence of the polymer.

Conclusion

In summary, our study has uncovered intricate electron transfer dynamics within the porphyrin, polymer, and MV^{2+} system. The presence of P4VPMe amplified $MV^{+\bullet}$ generation from ZnTPPS, underscoring the pivotal role of the polymer matrix. This effect is linked to the distinct aggregate states of ZnTPPS and TPPS within excess P4VPMe. Transient absorption studies revealed the dynamic electron transfer from the triplet state of ZnTPPS to MV^{2+}. Our research thus yielded valuable insights into electron transfer dynamics and their interplay with polymer matrices, potentially impacting photochemical and photophysical applications.

CRediT authorship contribution statement

Yilin CAO: Investigation, Formal analysis, Writing – review & editing, Writing – original draft, Investigation, Visualization, Data curation. **Hiraku SOTOME:** Writing – review, Research discussion, Investigation, Formal analysis, Visualization, Data curation, Methodology. **Yuichiro KOBAYASHI:** Writing – review, Research discussion. **Syoji ITO:** Writing – review, Research discussion, Methodology. **Hiroyasu YAMAGUCHI:** Writing – review, Conceptualization, Supervision, Resources, Methodology.

Declaration of Competing Interest

The authors declare that they have no known competing financial interests or personal relationships that could have appeared to influence the work reported in this paper.

Data availability

Data will be made available on request.

Acknowledgements

This work was partly supported by Iketani Science and Technology Foundation No.0351024-A, JSPS KAKENHI grant numbers JP21H01888, JP21H01889, JP21H04640, JP21H04964, JP21KK0092, JP22H00331, JP22H02145, JP22K19007, JP22K19066, JP23H01923, JP23H01926, JP23H03956, JP23H04877, and JST-Mirai Program Grant Number JPMJMI21G1. The authors wish to thank Prof.

Yoshinori TAKASHIMA and Asst. Prof. Ryohei IKURA of Osaka University for access to the GPC measurements.

Appendix A. Supplementary data.

Electronic Supplementary information (ESI) available: Synthesis and characterization of P4VPMe. Experimental procedures for irradiation.

Supplementary data to this article can be found online at.

References

[1] V. Balzani, A. Credi, M. Venturi, Photochemical conversion of solar energy, Chemsuschem 1 (2008) 26-58.

[2] M. Breuer, K. Rosso, J. Blumberger, Electron flow in multiheme bacterial cytochromes is a balancing act between heme electronic interaction and redox potentials, Proceedings of the National Academy of Sciences of the United States of America 111 (2014) 611-616.

[3] S. Rajak, N. Vu, P. Kaur, A. Duong, P. Nguyen-Tri, Recent progress on the design and development of diaminotriazine based molecular catalysts for light-driven hydrogen production, Coordination Chemistry Reviews 456 (2022) 214375.

[4] N. Yoshimura, M. Yoshida, A. Kobayashi, Efficient Hydrogen Production by a Photoredox Cascade Catalyst Comprising Dual Photosensitizers and a Transparent Electron Mediator, Journal of the American Chemical Society 145 (2023) 6035-6038.

[5] M. Wasielewski, Self-Assembly Strategies for Integrating Light Harvesting and Charge Separation in Artificial Photosynthetic Systems, Accounts of Chemical Research 42 (2009) 1910-1921.

[6] S. Fukuzumi, N. Fujioka, H. Kotani, K. Ohkubo, Y. Lee, W. Nam, Mechanistic Insights into Hydride-Transfer and Electron-Transfer Reactions by a Manganese(IV)-Oxo Porphyrin Complex, Journal of the American Chemical Society 131 (2009) 17127-17134.

[7] Y. Cao, T. Takasaki, S. Yamashita, Y. Mizutani, A. Harada, H. Yamaguchi, Control of Photoinduced Electron Transfer Using Complex Formation of Water-Soluble Porphyrin and Polyvinylpyrrolidone, Polymers 14 (2022) 1191.

[8] S. Frühbeisser, F. Gröhn, Catalytic Activity of Macroion-Porphyrin Nanoassemblies, Journal of the American Chemical Society 134 (2012) 14267-14270.

[9] A. Krieger, J. Werner, G. Mariani, F. Gröhn, Functional Supramolecular Porphyrin-Dendrimer Assemblies for Light Harvesting and Photocatalysis, Macromolecules 50 (2017) 3464-3475.

[10] R. Sadamoto, N. Tomioka, T. Aida, Photoinduced electron transfer reactions through dendrimer architecture, Journal of the American Chemical Society 118 (1996) 3978-3979.

[11] R. Wang, R. Qu, C. Jing, Y. Zhai, Y. An, L. Shi, Zinc porphyrin/fullerene/block copolymer micelle for enhanced electron transfer ability and stability, Rsc Advances 7 (2017) 10100-10107.

[12] X. Wang, L. Zhao, R. Ma, Y. An, L. Shi, Stability enhancement of ZnTPPS in acidic aqueous solutions by polymeric micelles, Chemical Communications 46 (2010) 6560-6562.
[13] T. Higashino, K. Kawamoto, K. Sugiura, Y. Fujimori, Y. Tsuji, K. Kurotobi, S. Ito, H. Imahori, Effects of Bulky Substituents of Push-Pull Porphyrins on Photovoltaic Properties of Dye-Sensitized Solar Cells, Acs Applied Materials & Interfaces 8 (2016) 15379-15390.
[14] A. Zhang, C. Li, F. Yang, J. Zhang, Z. Wang, Z. Wei, W. Li, An Electron Acceptor with Porphyrin and Perylene Bisimides for Efficient Non-Fullerene Solar Cells, Angewandte Chemie-International Edition 56 (2017) 2694-2698.
[15] D. Zhou, J. Wang, Z. Xu, H. Xu, J. Quan, J. Deng, Y. Li, Y. Tong, B. Hu, L. Chen, Recent advances of nonfullerene acceptors in organic solar cells, Nano Energy 103 (2022) 107802.
[16] C. Fu, X. Sun, G. Zhang, P. Shi, P. Cui, Porphyrin-Based Metal–Organic Framework Probe: Highly Selective and Sensitive Fluorescent Turn-On Sensor for M^{3+} (Al^{3+}, Cr^{3+}, and Fe^{3+}) Ions, Inorganic Chemistry 60 (2021) 1117-1124.
[17] S. Wirojsaengthong, D. Aryuwananon, W. Aeungmaitrepirom, B. Pulpoka, T. Tuntulani, A colorimetric paper-based optode sensor for highly sensitive and selective determination of thiocyanate in urine sample using cobalt porphyrin derivative, Talanta 231 (2021) 122371.
[18] L. Frolova, Y. Furmansky, A. Shestakov, N. Emelianov, P. Liddell, D. Gust, I. Visoly-Fisher, P. Troshin, Advanced Nonvolatile Organic Optical Memory Using Self-Assembled Monolayers of Porphyrin-Fullerene Dyads, Acs Applied Materials & Interfaces 14 (2022) 15461-15467.
[19] D. Xiang, X. Wang, C. Jia, T. Lee, X. Guo, Molecular-Scale Electronics: From Concept to Function, Chemical Reviews 116 (2016) 4318-4440.
[20] N. Lewis, Research opportunities to advance solar energy utilization, Science 351 (2016) 6271.
[21] X. Li, H. Lei, L. Xie, N. Wang, W. Zhang, R. Cao, Metalloporphyrins as Catalytic Models for Studying Hydrogen and Oxygen Evolution and Oxygen Reduction Reactions, Accounts of Chemical Research 55 (2022) 878-892.
[22] D. Nocera, The Artificial Leaf, Accounts of Chemical Research 45 (2012) 767-776.
[23] N. Maiti, S. Mazumdar, N. Periasamy, J- and H-aggregates of porphyrin-surfactant complexes: Time-resolved fluorescence and other spectroscopic studies, Journal of Physical Chemistry B 102 (1998) 1528-1538.
[24] C. Ruthard, M. Maskos, U. Kolb, F. Gröhn, Polystyrene Sulfonate-Porphyrin Assemblies: Influence of Polyelectrolyte and Porphyrin Structure, Journal of Physical Chemistry B 115 (2011) 5716-5729.
[25] A. Romeo, M. Castriciano, R. Zagami, G. Pollicino, L. Scolaro, R. Pasternack, Effect of zinc cations on the kinetics of supramolecular assembly and the chirality of porphyrin J-aggregates, Chemical Science 8 (2017) 961-967.
[26] I. Occhiuto, M. Castriciano, M. Trapani, R. Zagami, A. Romeo, R. Pasternack, L. Scolaro,

Controlling J-Aggregates Formation and Chirality Induction through Demetallation of a Zinc(II) Water Soluble Porphyrin, International Journal of Molecular Sciences 21 (2020) 4001.
[27] S. Logunov, M. Rodgers, Charge recombination reactions in self-assembled porphyrin-based ion-pair complexes, Journal of Photochemistry and Photobiology a-Chemistry 105 (1997) 55-63.
[28] T. Watanabe, K. Honda, Measurement of the extinction coefficient of the methyl viologen cation radical and the efficiency of its formation by semiconductor photocatalysis, Journal of Physical Chemistry 86 (1982) 2617-2619.
[29] M. Rougee, T. Ebbesen, F. Ghetti, R. Bensasson, Kinetics and mechanism of porphyrin-photosensitized reduction of methylviologen, Journal of Physical Chemistry 86 (1982) 4404-4412.
[30] J. Petersson, M. Eklund, J. Davidsson, L. Hammarström, Ultrafast Electron Transfer Dynamics of a Zn(II)porphyrin−Viologen Complex Revisited: S2 vs S1 Reactions and Survival of Excess Excitation Energy, Journal of Physical Chemistry B 114 (2010) 14329-14338.